Bulk and liquid – vapor interface of pyrrolidinium–based ionic liquids: A molecular simulation study

Xavier Paredes[1], Josefa Fernández[1], Agílio A.H. Pádua[2], Patrice Malfreyt[2,*], Friedrich Malberg[3], Barbara Kirchner[3], Alfonso S. Pensado[1,3,*]

[1]*Laboratorio de Propiedades Termofísicas, Departamento de Física Aplicada, Universidade de Santiago de Compostela, E-15782 Santiago de Compostela, Spain*

[2]*Institut de Chimie de Clermont-Ferrand, Equipe Thermodynamique et Interactions Moléculaires, Clermont Université, Université Blaise Pascal, BP 80026, 63171 Aubiere, France and CNRS, UMR6296 ICCF, BP 80026, F-63171 Aubière, France*

[3]*Mulliken Center for Theoretical Chemistry, Institut für Physikalische und Theoretische Chemie, Universität Bonn, Beringstr. 4+6, D-53115 Bonn, Germany*

[*]To whom correspondence should be addressed. Email: patrice.malfreyt@univ-bpclermont.fr, alfonso.pensado@thch.uni-bonn.de

Abstract

Using molecular dynamics simulations we have studied the structure of three 1-butyl-1-methylpyrrolidinium ionic liquids whose anions are triflate, bis(trifluoromethanesulfonyl)imide and tris(pentafluoroethyl)trifluorophosphate The structure of the bulk phase of the three ionic liquids has been interpreted using radial and spatial distribution functions, and structure factors, that allows us to characterize the morphology of the polar and non-polar domains present in this family of liquids. The size of the polar regions depends on the anion size, whereas the morphology of the non polar domains is anion independent. Furthermore, the surface ordering properties of the ionic liquids, and charge and density profiles, were also studied using molecular simulations. The surface tension of the liquid-vapor interfaces of these ionic liquids was also predicted from our molecular simulations. In addition, microscopic structural analysis of orientational ordering at the interface and density profiles along the direction normal to the interface suggest that the alkyl chains of the cation tend to protrude toward the vacuum, and the presence of the interface leads to a strong organization of the liquid phase in the region close to the interface. In the interfacial area, the polar regions of the ionic liquids are more structured than in the bulk phase, whereas the opposite behavior is observed for the non-polar regions.

Introduction

Room temperature ionic liquids (RTILs) are defined[1] as compounds constituted solely of ions with melting points lower than 373 K. The research on ionic liquids in its early stage was predominantly focused on their use as solvents, nowadays their perception within the scientific community has evolved, and they are considered as tunable multipurpose materials with a great variety of applications rather than just solvents[2-4]. Many ionic liquids present unique physicochemical properties, like very low volatility[5-7], high electrochemical[8,9] stability, wide liquid range[4,10], good electrical conductivity[11,12], and excellent ability to selectively dissolve different types of compounds[13,14]. Ionic liquids can be tailored to specific applications by fine-tuning the functional groups of the weakly coordinating organic cations and the inorganic/organic anion. There are many possible applications of ionic liquids that depend upon not only the bulk properties, but also upon the ionic liquid/gas surface. The use of ionic liquids as a medium for the synthesis of metallic nanoparticles[15,16], electrochemical applications[17,18], gas–storage[19,20], lubricants[21-23] or reaction media[1,24] will be strongly influenced by a better understanding of their bulk and interfacial properties. Thus, in his recent review Lovelock[25] emphasizes that the applications, for which there is dependence upon the interaction of different species with the ionic liquid/gas surface, cannot achieve the full extent of their potential without a profound understanding of the surface structure and properties.

A large number of studies appeared in the last years referring to imidazolium–based ionic liquids, just because these are the materials more used by synthetic chemists. In the last years, interest on pyrrolidinium–based ionic liquids has grown particularly amongst electrochemists, due to their wider electrochemical windows[26-28] and higher electrochemical stability when compared to imidazolium–based ILs. Santos et al.[29] have

performed a X-ray scattering study to analyze the bulk structure of the ILs [$C_nC_1$pyrr][NTf_2], (n = 4, 6, 8 and 10). First sharp diffraction peaks were found for the ILs with n larger than 6, a similar behavior was observed by Russina et al.[30] for the family [$C_nC_1$im][NTf_2]. Even if the imidazolium cation is planar and aromatic whereas the pyrrolidinium cation is nonplanar and nonaromatic, both families of ionic liquids display remarkably similar scattering patterns. Li et al.[31] performed a combined study, using X-ray scattering and molecular simulation to analyze the bulk structure (and its dependence with the temperature) of the ILs [$C_nC_1$pyrr][NTf_2], (n ranging from 3 to 10). The authors observe a good agreement between the experiments and the molecular simulation. MD results highlight the existence of a first (weak) diffraction peak for n=4. Men et al.[32] investigated the bulk phase of seven [$C_nC_1$pyrr][X] ionic liquids using X-ray photoelectron spectroscopy (XPS), to elucidate the binding energy for each ionic liquid. These authors relate the fact that the pyrrolidinium–based ionic liquids have a wider electrochemical window than their imidazolium-based counterparts with the observation that the carbon atom in position C2 of the imidazolium is more electropositive than any of the carbon atoms in the pyrrolidinium cation.

Men et al.[33] studied the surface chemistry of a series of four pyrrolidinium based ionic liquids, [$C_nC_1$pyrr][NTf_2] where n = 4–10, by angle resolved X-ray photoelectron spectroscopy (ARXPS), observing that as n increases, the surface composition becomes increasingly enriched with contributions from the linear alkyl substituents of the cation, which are significantly greater than that expected from the nominal stoichiometries. From inspection of this small homologous series of pyrrolidinium-based ionic liquids, it seems that the surface structure is analogous to that of [$C_nC_1$im][NTf_2] samples[34-37].

Molecular simulations have shown their ability to explore the structure of the bulk phase and the liquid-vacuum interface of ionic liquids[38-44]. Therefore in this work we

present MD studies of the bulk phase and the liquid-vacuum interface of the ionic liquids 1-butyl-1-methylpyrrolidinium triflate [C_4C_1pyrr][CF_3SO_3], 1-butyl-1-methylpyrrolidinium bis(trifluoromethanesulfonyl)imide [C_4C_1pyrr][NTf_2] and 1-butyl-1-methylpyrrolidinium tris(pentafluoroethyl)trifluorophosphate [C_4C_1pyrr][FAP]. This set of ionic liquids was chosen in order to understand the effect of changing the anion in the bulk phase structure, in the structure at the surface and the surface tension.

Simulation methodology

Potential model. The ionic liquids [C_4C_1pyrr][CF_3SO_3], [C_4C_1pyrr][NTf_2] and [C_4C_1pyrr][FAP] were represented by an all-atom force field[45,46], based on the OPLS_AA framework[47,48] but developed specifically for describing ionic liquids. The force field model contains the parameters required to simulate the 1-butyl-1-methylpyrrolidinium cation and the [CF_3SO_3], [NTf_2] and [FAP] anions (Figure 1). The functional form of the force field contains four kinds of potential energy: stretching of covalent bonds, bending of valence angles, torsion around dihedral angles, and nonbonded interactions. We consider that the nonbonded interactions are active between atoms of the same molecule separated by more than three bonds and between atoms of different molecules. The potential energy associated with bonds and angles is described by harmonic terms, dihedral torsion energy is represented by series of cosines, and nonbonded interactions are given by the Lennard–Jones sites and by Coulomb interactions (calculated using the Ewald summation method) between partial point charges placed on the atomic sites. Further details about the description of the force field can be found elsewhere[49].

Computational procedures. The bulk phases of the ionic liquids [C_4C_1pyrr][CF_3SO_3], [C_4C_1pyrr][NTf_2] and [C_4C_1pyrr][FAP] were simulated in periodic

cubic boxes containing 330, 280 and 230 ion pairs, respectively, using the molecular dynamics method implemented in the DL_POLY package[50]. The initial configurations were lattices with low density. Equilibrations starting from the low-density arrangement of ions took around 2 ns, at constant *NpT* and T = 423 K, with a timestep of 2 fs. Simulation runs of 2 ns were performed once the equilibrium density was obtained. The lengths of the sides of the simulation boxes at the final densities are around 52 Å. Additionally, for the analysis of the free surfaces of the ionic liquid, we have considered rectangular parallelepiped simulation boxes of dimensions $L_xL_yL_z$ (with L_x=L_y) containing 660 ion pairs of the ionic liquid [C_4C_1pyrr][CF_3SO_3], 560 ion pairs of the IL [C_4C_1pyrr][NTf_2] and 460 ion pairs of the IL [C_4C_1pyrr][FAP] for a total of around 25000 atoms in the simulated systems. Periodic boundary conditions were applied in the three directions of space. The direction normal to the surface of the ionic liquid was elongated (300 Å) so that the liquid slab occupies ~120 Å in the middle of the simulation box with two equivalent liquid-vacuum interfaces. The systems were simulated via molecular dynamics using the DL_POLY program[50] at 423 K. The system was coupled to Nosé-Hoover thermostats (constant NVT). The integration time step was 2 fs. Initial configurations were constructed by placing together two cubic boxes from the previous step. Equilibrations starting from this arrangement of ions took around 1 ns (N*p*T), after which the systems were run for 1 ns allowing the interface to equilibrate. Then, a production run of 2 ns was executed. As expected, no detectable vapor phase was observed during the simulations. We calculated profiles of typical properties as a function of *z* (as the geometry of the system shows heterogeneity along the axis normal to the interface, *z* axis) by splitting the cell into slabs of width Δz.

Several methods can be used to compute the surface tension from molecular simulations. The methods[51-53] used most frequently consider the mechanical route

definition and relate the surface tension to the components of the pressure tensor. The Kirkwood and Buff[53] expression evaluates the components of the pressure tensor as a function of the derivative of the intermolecular potential. The method proposed by Irving and Kirkwood[52] is based upon the notion of the force across a unit area and profits of expressing the local components of the pressure tensor along the direction normal to the interface. The IK approach allows us to check that the interfaces are well stabilized and exhibit features in line with the mechanical equilibrium of planar interfaces. Full details of the calculation methods, including the treatment of long-range corrections, can be found elsewhere[40,41].

Results and discussion

Bulk phase. Wang and Voth[54], using a multiscale coarse-graining (MS-CG) method, and Canongia Lopes and Pádua[38], using an all-atom potential model, reported the existence of a nanometer-scale structuring in imidazolium-based ionic liquids (from $[C_2C_1im]^+$ to $[C_{12}C_1im]^+$) corresponding to a segregation of polar and non-polar domains. Triolo and coworkers[30,44,55-58] provided experimental evidence, using X-Ray diffraction, of the existence of a nanoscale organization in the ionic liquids of five families based in $[C_nC_1im]^+$ cations and $[PF_6]^-$, $BF_4]^-$, $[Cl]^-$, $[NTf_2]^-$ or $[C_mSO_4]^-$ anions. Recently, Paredes et al.[43] using molecular simulation have found that nanosegregation also occurs in the family $[C_2C_1im][C_nSO_4]$ (n = 2, 4, 6 and 8). This segregation into polar (ionic) and non-polar spatial domains is important to define the solvation characteristics of ionic liquids[59,60], through effects of this dual structure and also through the types of interaction with polar and non-polar solutes. Recent experimental[61] and molecular simulation investigations[42] have shown that the presence of specific functionalities in the side chain of the imidazolium cations modifies the morphology of the polar and non-polar domains, but the characteristic nanosegregation is kept. X-ray

scattering studies and molecular simulations have indicated[31] that the IL $[C_4C_1pyrr][NTf_2]$ also presents a nanosegregation between polar and non-polar domains. We analyze here the influence of the anion in the microscopic structure for three ILs based on the $[C_4C_1pyrr]^+$ cation. The three carbon atoms at the end of the alkyl chains of the cations, together with their bonded hydrogen atoms, constitute the regions considered to be of low charge density, whereas the atoms of the pyrrolidinium cycle plus the atoms bounded to these, including the hydrogen atoms bonded to the first carbon of the alkyl chain, and all the atoms of the anions constitute the regions considered to be of high charge density. The justification for such a division is illustrated in the electrostatic surface potential plot depicted by Figure 2. The morphology of the polar and non-polar regions for the studied pyrrolidinium-based ionic liquids is illustrated in Figure 3, where the high charged regions were colored in blue and low-charge density regions in yellow. It is clear that the tail groups aggregate and form several spatially heterogeneous domains. The relative sizes of the non-polar domains in the three ionic liquids analyzed remains unchanged, whereas the size of the polar domains is strongly affected by the anion (Figure 3). A quantitative description of the nanostructure of the studied ionic liquids can be performed by means of the Radial Distribution Functions (RDFs) and static structure factors. Figure 4 depicts the RDFs between several representative atoms of the anions and cations, which show several remarkable features. We observe a strong correlation between the nitrogen atom of the pyrrolidinium cation and the anions, especially with $[CF_3SO_3]^-$ and $[NTf_2]^-$ for which the coordination to the cation (see panels a)-d) of Figure 4) occurs preferentially via the oxygen atoms of the anions (these atoms carry the most negative charge).

The situation is slightly more complex in the case of the $[FAP]^-$ anion, for which the coordination occurs preferentially via the fluoride atoms directly bonded to the

phosphorus and also via the terminal fluoride atoms of the perfluoroethyl chains. The peaks in the RDFs are more intense in the case of the IL $[C_4C_1pyrr][CF_3SO_3]$, the small size of the anions makes them easier to be closely packed in the neighborhood of the cation. Nevertheless an interesting feature appears when the second solvation shell is observed, namely the position of the second peak in the RDFs is shifted towards larger distances when the size of the anion is increased. Another interesting feature is that the terminal atoms of the $[C_4C_1pyrr]^+$ cations are found with a high probability at close distances from each other, which is a sign of alkyl-chain aggregation. The position of the peak is almost unaffected when the size of the anion increases; its intensity follows the trend $[C_4C_1pyrr][CF_3SO_3] > [C_4C_1pyrr][NTf_2] \approx [C_4C_1pyrr][FAP]$. Even in the case of the voluminous $[FAP]^-$ anion the non-polar chains of the cations stick together, forming the non-polar domains visualized in the snapshots of Figure 3.

To characterize the length scales of the polar and nonpolar regions, we can use the static partial structure factors, $s_{ij}(k)$ corresponding to the partial RDFs, $g_{ij}(r)$, that are defined by a Fourier transform according to equation 1, where ρ is the number density of the atomic sites considered.

$$s_{ij}(k) = 1 + \frac{4\pi\rho}{k} \int_0^\infty [g_{ij}(r) - 1] r \sin(kr) dr \quad (1)$$

The results for the partial structure factors of several representative sites of the polar and non-polar regions are presented in Figure 5. Concerning the structure factors of the terminal carbon atom of the side chain, the most remarkable features are the strong peaks in the region between 0.56 and 0.64 $Å^{-1}$. The peak wavenumbers corresponding to the length scales are presented in Table 1. The results suggest that the sizes of the non-polar regions are only slightly affected by the increase of the size of the anion. A slightly more interesting picture can be observed if we represent the partial

structure factors of the nitrogen atom of the pyrrolidinium cation. We observe the existence of a first peak at 0.95 $Å^{-1}$ corresponding to a wavelength λ = 6.6 Å for the IL $[C_4C_1pyrr][CF_3SO_3]$, at 0.84 $Å^{-1}$ (λ = 7.5 Å) for the IL $[C_4C_1pyrr][NTf_2]$ and at 0.78 $Å^{-1}$ (λ = 8.1 Å) for the IL $[C_4C_1pyrr][FAP]$, reflecting the characteristic distances between successive neighbor shells in the liquid structure, that depend on the type of anion, as previously was pointed out experimentally by Russina et al.[30] The existence of prepeaks in the structure factors indicates the presence of characteristic lengths that are larger than first-neighbor ion-ion contacts. Ionic liquids with alkyl side chains of intermediate length show the presence of such prepeaks, as it was previously observed[30,39,44,5558,61-69] using both experiments and molecular simulation. Such prepeaks, whose origin has been analyzed recently in great detail[66,67], indicate the aggregation of the chains into nonpolar domains, while the charged head groups of the ions keep in close contact. Margulis and coworkers have extensively studied the origin of such prepeaks.

Panel a) of Figure 5 shows secondary peaks at 0.5 $Å^{-1}$ corresponding to a wavelength of around 12.6 Å for the IL $[C_4C_1pyrr][CF_3SO_3]$, at 0.43 $Å^{-1}$ (λ = 15.1 Å) for the IL $[C_4C_1pyrr][NTf_2]$ and at 0.32 $Å^{-1}$ (λ = 19.6 Å) for the IL $[C_4C_1pyrr][FAP]$. The polar domain length scales in the investigated ionic liquids are quantitatively different, as can be visualized by comparing the results of Figure 5 with the snapshots of Figure 3. The different morphology of the nanoscale domains in these ionic liquids can influence the solvation of different species, and so probably also the performance of these liquids as reaction or separation media. The results for the IL $[C_4C_1pyrr][NTf_2]$ presented here agree quantitatively with the molecular simulation results of Li et al.[31]

Ionic liquid-gas interface. Figure 6 depicts the number density profile of the most representative atoms of the cation and anions. The alkyl side chains of the cations

tend to protrude towards the vacuum, in agreement with experimental results[33,70,71]. Deep minima for the number density of the atoms of the side chain are observed in the denser region (this aspect is less marked in the case of the IL [C_4C_1pyrr][FAP]). The oxygen atoms of the $[CF_3SO_3]^-$ and $[NTf_2]^-$ anions (those atoms carry the most negative charge on the anion) are found in the same region as the pyrrolidinium ring. The terminal CF_3 groups of the $[CF_3SO_3]^-$ point also towards the vacuum. Concerning the $[NTf_2]^-$ anion, the fluorine atoms are the outermost ones, whereas the nitrogen atoms are placed deeper into the liquid. Some remarkable features are observed for the IL [C_4C_1pyrr][FAP]: i) The local density of the side chains of the cation in the most outer region is much lower than for the other studied ILs. ii) A denser sub-surface region as clearly appears in the case of the ILs [C_4C_1pyrr][CF_3SO_3] and [C_4C_1pyrr][NTf_2] is not observed for the IL based in the $[FAP]^-$ anion. iii) The different atoms of the bulk $[FAP]^-$ anion are present in the interfacial region. This can be related to the hydrophobic character of the anion and to the difficulty to compactly pack such voluminous anion at the interface. The simulation snapshot of the left side of Figure 7 shows a view looking onto the surface of the studied ionic liquids. It can be seen that the alkyl chains do not cover the surface completely for the three ionic liquids. This implies therefore, that the polar parts of the ionic liquids are accessible from above the surface, with this effect being more intense when the size of the anion increases. The structure of the polar and non-polar regions of the ionic liquid is not strongly affected by the presence of a free surface[40,41,43], so the ionic liquid keeps its characteristic nano-scale heterogeneity.

Figure 8 depicts the plots of the orientational ordering parameter, defined as the average of the second Legendre polynomial:

$$\langle P_2(\theta)\rangle = \left\langle \frac{1}{2}(3\cos^2\theta - 1)\right\rangle \quad (2)$$

In Eq. 2, θ is taken as the angle between a specific direction vector in the molecule-fixed frame and the surface normal *z*. The Legendre polynomial functions enable us to investigate the range and extent of orientation preferences at the interface. $P_2(\theta)$ ranges from 1 to -0.5. A value of 1 implies that the two considered vectors are parallel, whereas a value of -0.5 indicates that they are perpendicular. We observe that the pyrrolidinium ring adopts in the three investigated ionic liquids preferential orientations perpendicular to the interface, confirming the results presented in the density profiles in Figure 5 (the nitrogen atom N1 is located closer to the vacuum-liquid surface than the atoms C3,4). Nevertheless, for the IL $[C_4C_1pyrr][FAP]$ the structure at the vacuum-liquid interface is less ordered than for the other two investigated ionic liquids, in agreement with the previous results for the density profiles. The presence of a bulky, voluminous anion strongly distorts the ordering in the ionic liquid caused by the presence of an explicit interface. The side chains of the cations form, in average, an angle between 25º and 40º with the normal to the interface, in good agreement with the observations of Aliaga et al.[71] using Sum Frequency Generation experiments. The analysis of the preferential orientation of the different anions shows several remarkable features. The ST-CT vector of the $[CF_3SO_3]^-$ forms an angle of around 30º with the normal vector to the surface. The S-S vector of the $[NTf_2]^-$ anion is orientated forming an angle of 60º with the normal vector to the surface, in good agreement with previous results[72] for several ionic liquids linked to the $[NTf2]^-$ anion. For the $[FAP]^-$ anion, the vector connecting the phosphorous and the fluoride atoms, and the vector P-C3F show preferential orientations with angles between 20º and 40º with the normal vector to the surface, highlighting that different orientations of the anion are present, that results on a more disordered structure at the vacuum-liquid surface.

The charge density profiles for [C_4C_1pyrr][CF_3SO_3], Panel a), and [C_4C_1pyrr][NTf_2], Panel b) of Figure 9 exhibit a high peak at the interface for both ions, which indicate that charge for both the cation and anion is enhanced at the interfacial region. This peak in the interfacial region is lower for the IL [C_4C_1pyrr][FAP]. For all the studied ILs there is a small excess of negative charge in the outermost interfacial region. The fluctuations of the charge density profiles in the interfacial region occurs in typical sizes smaller than the size of the single ions, showing that there is no electrical-double-layer of the size of the ions on the liquid-vacuum interface of the ionic liquid, just a weak segregation between cations and anions occurs at the interface. The electrostatic potential changes when crossing the surface of a liquid containing polar or charged entities. From the charge density profiles it is possible to evaluate the electrostatic potential Φ using the Gauss' theorem:

$$\frac{\mathrm{d}\Phi}{\mathrm{d}z_k} = -\frac{1}{\varepsilon_0}\int_{-\infty}^{z_k} \rho_q(z')\,\mathrm{d}z' \qquad (3)$$

where $\rho_q(z')$ is the charge density at the position z'. Panel d) of Figure 9 shows the variation of the potential across the direction normal to the interface. Bresme et al.[73] considered an ionic liquid consisting of spherical rigid ions interacting through the so-called "soft primitive model" (SPM), and they observed that ion size asymmetry results in charge separation at the liquid–vapour interface and therefore in a local violation of the electroneutrality condition. The authors observed that an increase in size asymmetry results in an increase of the potential. The electrostatic potential[41] for [C_6C_1im][NTf_2] is ~0.2 V. For [C_2C_1im][BF_4], [C_2OHC_1im][BF_4], [C_2C_1im][BF_4] and [C_2OHC_1im][BF_4] the potential[40] ranges from -0.15 to -0.35 V. For [C_2C_1im][C_2SO_4] the electrostatic potential[43] is around -0.45 V whereas for [C_2C_1im][C_8SO_4] is around -0.55 V. Relative to the vacuum, the potential for [C_4C_1pyrr][NTf_2] and [C_4C_1pyrr][FAP] is positive,

whereas for $[C_4C_1pyrr][CF_3SO_3]$ the potential is compatible with zero. The results presented here, together with those previously obtained for other ILs suggest that the electrostatic potential can be adjusted by selecting a combination of cation and anion, being the influence of the selected anion larger. It is clear that the local ordering of the ions at the surface, the effective packing of the anion and cation in the interfacial region, together with the molecular structure of the ions are key-parameters that control the values of the electrostatic potential at the surface.

To analyze the effect of the explicit interface on the structure of the ionic liquids, we calculated zone-resolved tangential pair distribution functions (TRDF) that will allow us to analyze the lateral structure of the interface. The TRDFs are defined by:

$$g_{ij}(r) = \frac{\sum_{i,j} \delta(r - r_{ij})}{2\pi r\, dr\, \rho_{region}\, \Delta z}; \quad z_{ij} < \Delta z \tag{4}$$

where ρ_{region} is the average number density in each region which normalizes the corresponding TRDF to unity at infinite distance, and $r_{ij} = (x_{ij}^2 + y_{ij}^2)^{1/2}$ is a two-dimensional distance, parallel to the plane of the surface. Δz = 5 Å is chosen to achieve significant statistical averages.

Figure 10 depicts the TRDFs between several representative atoms of the investigated ionic liquid. The TRDFs between the nitrogen atom N1 of the pyrrolidinium ring and the oxygen atoms of the $[CF_3SO_3]^-$ anion are quite similar in the interfacial region and in the bulk; just the second peak in the TRDF at the interface is larger than in the bulk. We observe that the TRDFs between the nitrogen atom N1 of the pyrrolidinium ring and the oxygen atoms of the $[NTf_2]^-$ anion and the fluorine atom and the terminal carbon atom of the perfluoroethyl chain of the $[FAP]^-$ anion present higher peaks in the interfacial region compared with the bulk, suggesting a more ordered liquid phase in the

interfacial region. The most remarkable feature is the loss of the correlation in the interfacial region between the terminal carbon atoms of the alkyl side chains of the cations and also between the perfluoroalkyl chains of the anions. The outer region of the interface is composed mainly of the side chains of the anions, but their correlation is weak, as can be also observed in the snapshots of the simulation boxes presented in Figure 7.

The values of the surface tension for the three considered ionic liquids are presented in Table 3, and are calculated using the Kirkwood–Buff[53] (KB) and Irving–Kirkwood[52] (IK) expressions. Both methods provide results that are in quite good agreement. Panel a) of Figure 11 shows the profiles of the surface tension for the ionic liquid $[C_4C_1pyrr][NTf_2]$ across the direction normal to the interface; similar behavior is observed for the other two ionic liquids. The contributions to the surface tension for a system in mechanical equilibrium should come from the interfacial regions and not from the isotropic bulk region[74-77]. As it is required for a system in mechanical equilibrium, the profiles of pseudo-local surface tension should increase in a similar way in the two interfacial regions, and remain constant in the bulk phase. The dispersion-repulsion contribution to the surface tension (calculated from the Irving-Kirkwood approach) is negative, whereas the electrostatic contribution is positive, a common behavior of ionic liquids. We present in panel b) of Figure 11 the contribution of the long-range correction to the surface tension for $[C_4C_1pyrr][CF_3SO_3]$. Again, there is no contribution of the long-range correction to the surface tension coming from the bulk, since the integral of $\gamma_z(z_k)$ is flat in this region. The long-range corrections[78], γ_{LRC}, to the surface tension account for around 10% of the total value (see Table 2) and this underlines the need of considering this correction carefully. It is possible to relate the surface tension of the ionic liquids to the structure at the free surface. The force field

used in this work was not adjusted to surface properties; therefore, the calculation of surface tension is also a test of the transferability of the force field.

Fletcher et al.[79] have measured the surface tension of the IL [C_4C_1pyrr][FAP] at 293 K using the Du Noüy ring, finding a value of 38 mN·m^{-1}. Kolbeck et al.[80] investigated the surface tension of the IL [C_4C_1pyrr][NTf_2] from 293 to 298 K using the pending drop method, obtaining values in the range 32.7 to 32.3 mN·m^{-1}. Jin et al.[81] obtained for this IL a value of the surface tension of 33 mN·m^{-1} at 293 K. Shamsipur et al.[82], using the Du Noüy ring method report experimental values of the surface tension for the IL [C_4C_1pyrr][NTf_2] from 283 to 363 K, being in the range from 34.5 to 33 mN·m^{-1}. Using the same method, Carvalho et al.[83] have obtained that the surface tension for the same IL from 293 to 343 K ranges from 34.9 to 32 mN·m^{-1}. No surface tension data is available in the literature for the IL [C_4C_1pyrr][CF_3SO_3], nevertheless for imidazolium based IL, with a common cation, the surface tension values of the IL based in the $[CF_3SO_3]^-$ and $[NTf_2]^-$ anions are quite similar[84]. As the temperature range of the experimental measurements and the simulations performed here do not overlap, it is difficult to perform comparisons between the data, nevertheless we can roughly conclude that the atomistic force field and the simulation techniques used in the present work are able to predict the surface tension of ionic liquids within a deviation of ±10%.

According to the Langmuir principle, only the parts of the ions that are at the outer surface will primarily contribute to the surface tension values[85]. The similar structure at the liquid-vacuum interface for the ILs with the $[CF_3SO_3]^-$ and $[NTf_2]^-$ anions presented here is in agreement with the trends of the surface tension observed from the molecular simulations. For the IL [C_4C_1pyrr][FAP] the presence of a voluminous anion incites a lack of ordering at the surface, which is enriched with the most charged part of the ions, as it can be observed in the density profiles depicted in Figure 6, leading to larger values

of the surface tension (see Table 2). Pensado et al.[40] demonstrate that the inclusion of a terminal hydroxyl group at the end of the side chain of imidazolium based ILs distorts the structure at the liquid-vacuum interface, leading to larger values of the surface tension, a similar behavior as the observed here for the IL [C_4C_1pyrr][FAP].

Conclusions

The structure of the bulk phase and the vacuum-liquid interface of three pyrrolidinium based ionic liquids, with a common cation, has been studied using molecular simulations. The studied liquids show segregation between polar and non-polar domains, where the morphology of the non-polar regions is independent of the specific anion. Increasing the size of the anion leads to an increase of the characteristic sizes of the polar domains. The analysis of the vacuum-liquid interface shows an enrichment of the surface composition with the alkyl side chains of the cations. The presence of a discontinuity in the local density leads to a small charge segregation at the surface, being this effect less intense for the IL with the $[FAP]^-$ anion, as this voluminous anion incites a lack of ordering in the surface. From the charge distribution it is possible to determine the electrostatic potential, observing a clear dependence of this magnitude with the anion. The analysis of the tangential pair distribution functions shows that in the interfacial area, the polar regions of the ionic liquids are more structured than in the bulk phase, whereas the opposite behavior is observed for the non-polar regions.

Acknowledgements

This work was supported by the Spanish Science and Technology Ministry (CTQ2008-6498-C02-01 and CTQ2011-23925 projects) and the DFG, in particular by the projects KI-768/7-1 and KI-768/5-3 from the SPP-IL program. The participation of ASP was

made possible by a post-doctoral fellowship granted by the DFG through the SPP-IL program. Computer time from the “Centro de Supercomputación de Galicia” (CESGA) is acknowledged gratefully.

References

(1) Hallett, J. P.; Welton, T. *Chem. Rev.* **2011**, *111*, 3508-3576.
(2) Welton, T. *Chem. Rev.* **1999**, *99*, 2071-2083.
(3) Plechkova, N. V.; Seddon, K. R. *Chem. Soc. Rev.* **2008**, *37*, 123-150.
(4) Wasserceheid, P.; Welton, T. *Ionic Liquids in Synthesis, Second Edition*; WILEY-VCH, 2008.
(5) Earle, M. J.; Esperança, J. M. S. S.; Gilea, M. A.; Canongia Lopes, J. N.; Rebelo, L. P. N.; Magee, J. W.; Seddon, K. R.; Widegren, J. A. *Nature* **2006**, *439*, 831-834.
(6) Rebelo, L. P. N.; Canongia Lopes, J. N.; Esperança, J. M. S. S.; Filipe, E. *J. Phys. Chem. B* **2005**, *109*, 6040-6043.
(7) Zaitsau, D. H.; Kabo, G. J.; Strechan, A. A.; Paulechka, Y. U.; Tschersich, A.; Verevkin, S. P.; Heintz, A. *J. Phys. Chem. A* **2006**, *110*, 7303-7306.
(8) Weingarth, D.; Czekaj, I.; Fei, Z.; Foelske-Schmitz, A.; Dyson, P. J.; Wokaun, A.; Koetz, R. *J. Electrochem. Soc.* **2012**, *159*, H611-H615.
(9) Weingarth, D.; Foelske-Schmitz, A.; Koetz, R. *J. Power Sour.* **2013**, *225*, 84-88.
(10) Holbrey, J. D.; Seddon, K. R. *J. Chem. Soc.. Dalton Trans.* **1999**, 2133-2140.
(11) MacFarlane, D. R.; Forsyth, M.; Izgorodina, E. I.; Abbott, A. P.; Annat, G.; Fraser, K. *Phys. Chem. Chem. Phys* **2009**, *11*, 4962-4967.
(12) Vila, J.; Varela, L. M.; Cabeza, O. *Electrochimica Acta* **2007**, *52*, 7413-7417.
(13) Blesic, M.; Canongia Lopes, J. N.; Costa Gomes, M. F.; Rebelo, L. P. N. *Phys. Chem. Chem. Phys* **2010**, *12*, 9685-9692.
(14) Canongia Lopes, J. N.; Costa Gomes, M. F.; Pádua, A. A. H. *J. Phys. Chem. B* **2006**, *110*, 16816-16818.
(15) Wender, H.; Andreazza, M. L.; Correia, R. R. B.; Teixeira, S. R.; Dupont, J. *Nanoscale* **2011**, *3*, 1240-1245.
(16) Wender, H.; Migowski, P.; Feil, A. F.; de Oliveira, L. F.; Prechtl, M. H. G.; Leal, R.; Machado, G.; Teixeira, S. R.; Dupont, J. *Phys. Chem. Chem. Phys* **2011**, *13*, 13552-13557.
(17) MacFarlane, D. R.; Pringle, J. M.; Howlett, P. C.; Forsyth, M. *Phys. Chem. Chem. Phys* **2010**, *12*, 1659-1669.
(18) Simons, T. J.; Torriero, A. A. J.; Howlett, P. C.; MacFarlane, D. R.; Forsyth, M. *Electrochem. Commun.* **2012**, *18*, 119-122.
(19) Janiczek, P.; Kalb, R. S.; Thonhauser, G.; Gamse, T. *Sep. Purif. Technol.* **2012**, *97*, 20-25.
(20) Althuluth, M.; Kroon, M. C.; Peters, C. J. *Ind. Eng. Chem. Res.* **2012**, *51*, 16709-16712.
(21) Jimenez, A. E.; Bermudez, M. D. *Tribol. Lett.* **2010**, *37*, 431-443.
(22) Jimenez, A. E.; Bermudez, M. D. *Tribol. Lett.* **2010**, *40*, 237-246.

(23) Jimenez, A. E.; Bermudez, M.-D. *Tribol. Lett.* **2009**, *33*, 111-126.

(24) Tietze, A. A.; Heimer, P.; Stark, A.; Imhof, D. *Molecules* **2012**, *17*, 4158-4185.

(25) Lovelock, K. R. J. *Phys. Chem. Chem. Phys* **2012**, *14*, 5071-5089.

(26) Borgel, V.; Markevich, E.; Aurbach, D.; Semrau, G.; Schmidt, M. *J. Power Sour.* **2009**, *189*, 331-336.

(27) Hayyan, M.; Mjalli, F. S.; Hashim, M. A.; AlNashef, I. M.; Mei, T. X. *J. Ind. Eng. Chem.* **2013**, *19*, 106-112.

(28) O'Mahony, A. M.; Silvester, D. S.; Aldous, L.; Hardacre, C.; Compton, R. G. *J. Chem. Eng. Data* **2008**, *53*, 2884-2891.

(29) Santos, C. S.; Murthy, N. S.; Baker, G. A.; Castner, E. W., Jr. *J. Chem. Phys.* **2011**, *134*, 121101.

(30) Russina, O.; Triolo, A.; Gontrani, L.; Caminiti, R.; Xiao, D.; Hines, L. G., Jr.; Bartsch, R. A.; Quitevis, E. L.; Pleckhova, N.; Seddon, K. R. *J. Phys. Condens. Matter* **2009**, *21*,424121

(31) Li, S.; Banuelos, J. L.; Guo, J.; Anovitz, L.; Rother, G.; Shaw, R. W.; Hillesheim, P. C.; Dai, S.; Baker, G. A.; Cummings, P. T. J. Phys. Chem. Lett. **2012**, 3, 125-130.

(32) Men, S.; Lovelock, K. R. J.; Licence, P. *Phys. Chem. Chem. Phys* **2011**, *13*, 15244-15255.

(33) Men, S.; Hurisso, B. B.; Lovelock, K. R. J.; Licence, P. *Phys. Chem. Chem. Phys* **2012**, *14*, 5229-5238.

(34) Hammer, T.; Reichelt, M.; Morgner, H. *Phys. Chem. Chem. Phys* **2010**, *12*, 11070-11080.

(35) Lovelock, K. R. J.; Kolbeck, C.; Cremer, T.; Paape, N.; Schulz, P. S.; Wasserscheid, P.; Maier, F.; Steinrueck, H. P. *J. Phys. Chem. B* **2009**, *113*, 2854-2864.

(36) Maier, F.; Cremer, T.; Kolbeck, C.; Lovelock, K. R. J.; Paape, N.; Schulz, P. S.; Wasserscheidc, P.; Steinrueck, H. P. *Phys. Chem. Chem. Phys* **2010**, *12*, 1905-1915.

(37) Reinmöller, M.; Ulbrich, A.; Ikari, T.; Preiss, J.; Höfft, O.; Endres, F.; Krischok, S.; Beenken, W. J. D. *Phys. Chem. Chem. Phys* **2011**, *13*, 19526-19533.

(38) Canongia Lopes, J. N.; Pádua, A. A. H. *J. Phys. Chem. B* **2006**, *110*, 3330-3335.

(39) Macchiagodena, M.; Gontrani, L.; Ramondo, F.; Triolo, A.; Caminiti, R. *J. Chem. Phys.* **2011**, *134*, 114521.

(40) Pensado, A. S.; Costa Gomes, M. F.; Canongia Lopes, J. N.; Malfreyt, P.; Padua, A. A. H. *Phys. Chem. Chem. Phys.* **2011**, *13*.

(41) Pensado, A. S.; Malfreyt, P.; Pádua, A. A. H. *J. Phys. Chem. B* **2009**, *113*, 14708–14718.

(42) Pensado, A. S.; Padua, A. A. H.; Costa Gomes, M. F. *J. Phys. Chem. B* **2011**, *115*, 3942-3948.

(43) Paredes, X.; Fernandez, J.; Padua, A. A. H.; Malfreyt, P.; Malberg, F.; Kirchner, B.; Pensado, A. S. *J. Phys. Chem. B* **2012**, *116*, 14159-14170.

(44) Macchiagodena, M.; Ramondo, F.; Triolo, A.; Gontrani, L.; Caminiti, R. *J. Phys. Chem. B* **2012**, *116*, 13448-13458.

(45) Canongia Lopes, J. N.; Pádua, A. A. H. *J. Phys. Chem. B* **2004**, *108*, 16893-16898.

(46) Shimizu, K.; Almantariotis, D.; Costa Gomes, M. F.; Pádua, A. A. H.; Canongia Lopes, J. N. *J. Phys. Chem. B* **2010**, *114*, 3592-3600.

(47) Cornell, W. D.; Cieplak, P.; Bayly, C. I.; Gould, I. R.; Merz, K. M.; Fergusin, D. M.; Spellmeyer, D. C.; Fox, T.; Caldwell, J. W.; Kollman, P. A. *J. Am. Chem. Soc.* **1995**, *117*, 5179-5197.

(48) Jorgensen, W. L.; Maxwell, D. S.; Tirado-Rives, J. *J. Am. Chem. Soc.* **1996**, *118*, 11225-11236.

(49) Canongia Lopes, J. N.; Pádua, A. A. H. *Theor. Chem. Acc.* **2012**, *131*, 1129.

(50) Smith, W.; Todorov, I. DL_POLY Classic Molecular Simulation Package, 2012.

(51) Gloor, G. J.; Jackson, G.; Blas, F. J.; De-Miguel, E. *J. Chem. Phys.* **2005**, *123*, 134703/134701-134719.

(52) Irving, J. H.; Kirkwood, J. G. *J. Chem. Phys.* **1950**, *18*, 817-829.

(53) Kirkwood, J. G.; Buff, F. P. *J. Chem. Phys.* **1949**, *17*, 338-343.

(54) Wang, Y.; Voth, G. A. *J. Am. Chem. Soc.* **2005**, *127*, 12192-12193.

(55) Russina, O.; Triolo, A.; Gontrani, L.; Caminiti, R. *J. Phys. Chem. Lett.* **2012**, *3*, 27-33.

(56) Triolo, A.; Russina, O.; Bleif, H.-J.; Di Cola, E. *J. Phys. Chem. B* **2007**, *111*, 4641-4644.

(57) Triolo, A.; Russina, O.; Fazio, B.; Triolo, R.; Di Cola, E. *Chem. Phys. Lett.* **2008**, *457*, 362-365.

(58) Russina, O.; Triolo, A. *Faraday Discuss.* **2012**, *154*, 97-109.

(59) Gutel, T.; Santini, C. C.; Philippot, K.; Padua, A. A. H.; Pelzer, K.; Chaudret, B.; Chauvin, Y.; Basset, J. M. *J. Mat. Chem.* **2009**, *19*, 3624-3631.

(60) Pádua, A. A. H.; Costa Gomes, M. F.; Canongia Lopes, J. N. *Acc. Chem. Res.* **2007**, *40*, 1087-1096.

(61) Triolo, A.; Russina, O.; Caminiti, R.; Shirota, H.; Lee, H. Y.; Santos, C. S.; Murthy, N. S.; Castner, E. W., Jr. *Chem. Commun.* **2012**, *48*, 4959-4961.

(62) Bowron, D. T.; D'Agostino, C.; Gladden, L. F.; Hardacre, C.; Holbrey, J. D.; Lagunas, M. C.; McGregor, J.; Mantle, M. D.; Mullan, C. L.; Youngs, T. G. A. *J. Phys. Chem. B* **2010**, *114*, 7760-7768.

(63) Deetlefs, M.; Hardacre, C.; Nieuwenhuyzen, M.; Padua, A. A. H.; Sheppard, O.; Soper, A. K. *J. Phys. Chem. B* **2006**, *110*, 12055-12061.

(64) Hardacre, C.; Holbrey, J. D.; Mullan, C. L.; Nieuwenhuyzen, M.; Youngs, T. G. A.; Bowron, D. T. *J. Phys. Chem. B* **2008**, *112*, 8049-8056.

(65) Hardacre, C.; Holbrey, J. D.; Mullan, C. L.; Youngs, T. G. A.; Bowron, D. T. *J. Chem. Phys.* **2010**, *133*.

(66) Annapureddy, H. V. R.; Kashyap, H. K.; De Biase, P. M.; Margulis, C. J. *J. Phys. Chem. B* **2010**, *114*, 16838-16846.

(67) Kashyap, H. K.; Hettige, J. J.; Annapureddy, H. V. R.; Margulis, C. J. *Chem. Commun*. **2012**, *48*, 5103-5105.

(68) Kashyap, H. K.; Santos, C. S.; Annapureddy, H. V. R.; Murthy, N. S.; Margulis, C. J.; Castner, E. W., Jr. *Faraday Discuss*. **2012**, *154*, 133-143.

(69) Kashyap, H. K.; Santos, C. S.; Daly, R. P.; Hettige, J. J.; Murthy, N. S.; Shirota, H.; Castner, E. W., Jr.; Margulis, C. J. *J. Phys. Chem. B* **2013**, *117*, 1130-1135.

(70) Lockett, V.; Sedev, R.; Harmer, S.; Ralston, J.; Horne, M.; Rodopoulos, T. *Phys. Chem. Chem. Phys* **2010**, *12*, 13816-13827.

(71) Aliaga, C.; Baker, G. A.; Baldelli, S. *J. Phys. Chem. B* **2008**, *112*, 1676-1684.

(72) Perez-Blanco, M. E.; Maginn, E. J. *J. Phys. Chem. B* **2010**, 11827-11837.

(73) Bresme, F.; González-Melchor, M.; Alejandre, J. *J. Phys.: Condens. Matter* **2005**, *17*, S3301-S3307.

(74) Biscay, F.; Ghoufi, A.; Goujon, F.; Lachet, V.; Malfreyt, P. *J. Chem. Phys.* **2009**, *130*.

(75) Biscay, F.; Ghoufi, A.; Lachet, V.; Malfreyt, P. *J. Phys. Chem. B* **2011**, *115*, 8670-8683.

(76) Ghoufi, A.; Goujon, F.; Lachet, V.; Malfreyt, P. *J. Chem. Phys.* **2008**, *128*.

(77) Neyt, J. C.; Wender, A.; Lachet, V.; Malfreyt, P. *J. Phys. Chem. C* **2012**, *116*, 10563-10572.

(78) Guo, M.; Lu, B. C.Y. *J. Chem. Phys.* **1998**, *109*, 1134-1140.

(79) Fletcher, S. I.; Sillars, F. B.; Hudson, N. E.; Hall, P. J. *J. Chem. Eng. Data* **2010**, *55*, 778-782.

(80) Kolbeck, C.; Lehmann, J.; Lovelock, K. R. J.; Cremer, T.; Paape, N.; Wasserchеid, P.; Fröba, A. P.; Maier, F.; Steinrueck, H. P. *J. Phys. Chem. B* **2010**, *114*, 17025-17036.

(81) Jin, H.; O'Hare, B.; Dong, J.; Arzhantsev, S.; Baker, G. A.; Wishart, J. F.; Benesi, A. J.; Maroncelli, M. *J. Phys. Chem. B* **2008**, *112*, 81-92.

(82) Shamsipur, M.; Beigi, A. A. M.; Teymouri, M.; Pourmortazavi, S. M.; Irandoust, M. *J, Mol. Liq.* **2010**, *157*, 43-50.

(83) Carvalho, P. J.; Neves, C. M. S. S.; Coutinho, J. A. P. *J. Chem. Eng. Data* **2010**, *55*, 3807-3812.

(84) Tariq, M.; Freire, M. G.; Saramago, B.; Coutinho, J. A. P.; Canongia Lopes, J. N.; Rebelo, L. P. N. *Chem. Soc. Rev.* **2012**, *41*, 829-868.

(85) Oliveira, M. B.; Dominguez-Perez, M.; Freire, M. G.; Llovell, F.; Cabeza, O.; Lopes-da-Silva, J. A.; Vega, L. F.; Coutinho, J. A. P. *J. Phys. Chem. B* **2012**, *116*, 12133-12141.

FIGURE 1

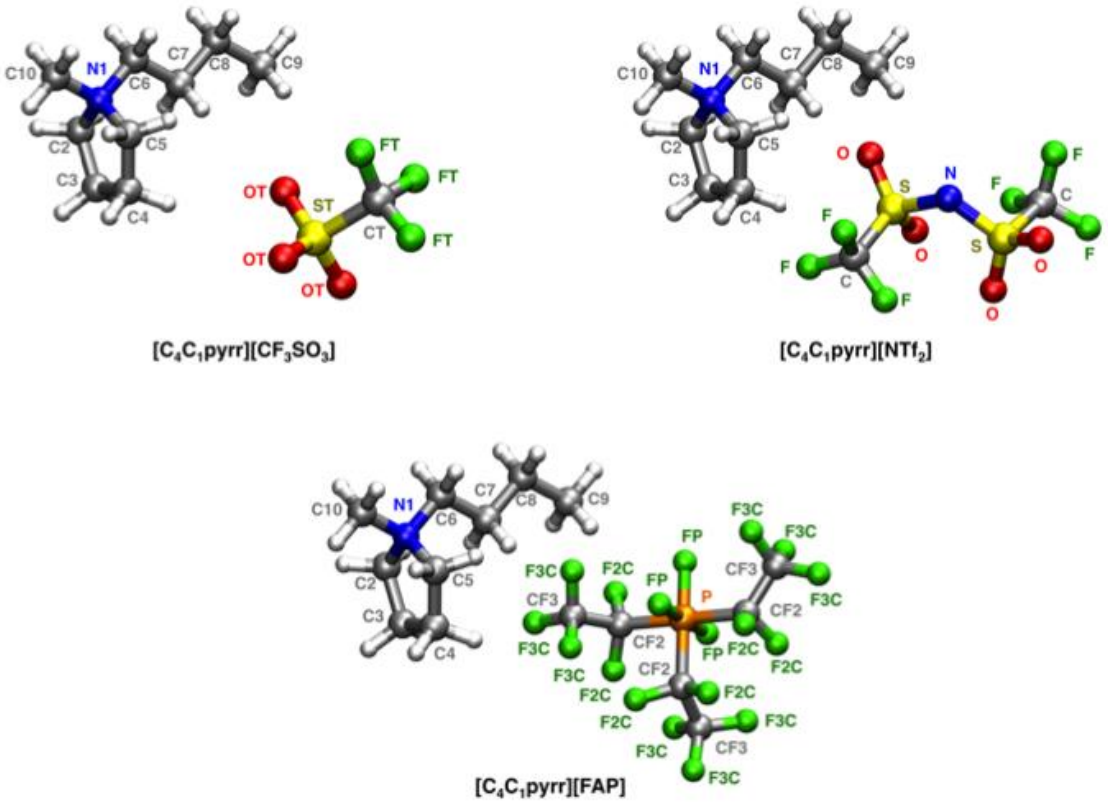

Figure 1. Adopted nomenclature for the sites of the ionic liquids 1-butyl-1-methylpyrrolidinium triflate, 1-butyl-1-methylpyrrolidinium bis(trifluoromethanesulfonyl)imide and 1-butyl-1-methylpyrrolidinium tris(pentafluoroethyl)trifluorophosphate.

FIGURE 2

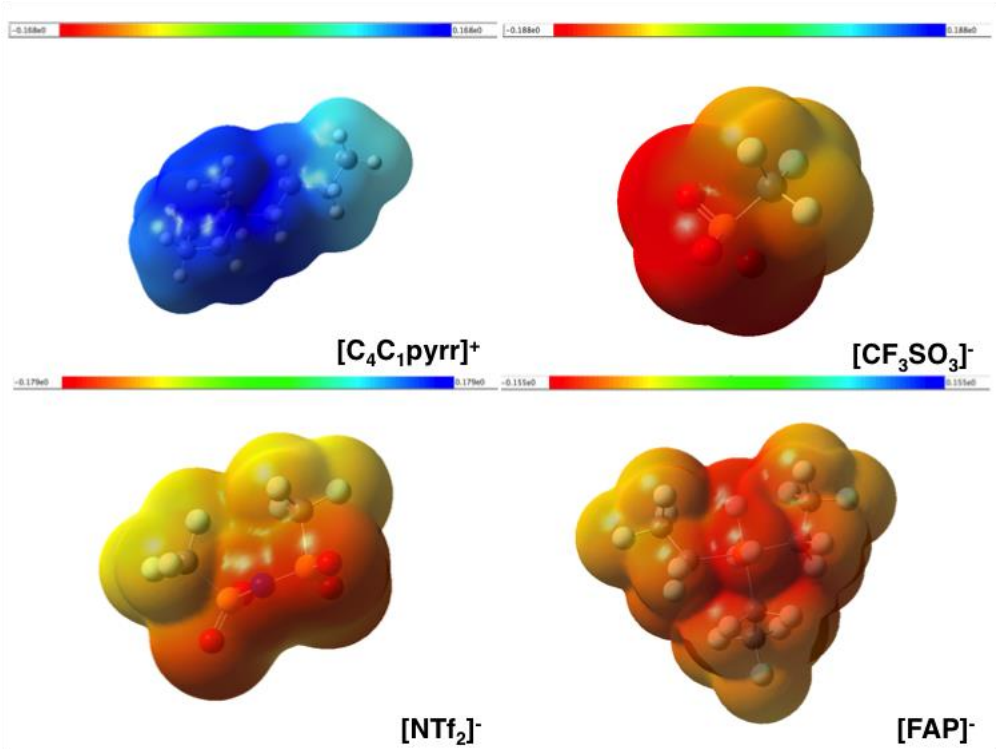

Figure 2. Mapping of the electrostatic potential onto an isoelectronic density surface obtained *ab initio* at the MP2 level (darker blue shades represent more positive regions and darker red colors indicate more negative regions) in the $[C_4C_1pyrr]^+$ cation and $[CF_3SO_3]^-$, $[NTf_2]^-$ and $[FAP]^-$ anions. Details of the calculations can be found in the literature[45].

FIGURE 3

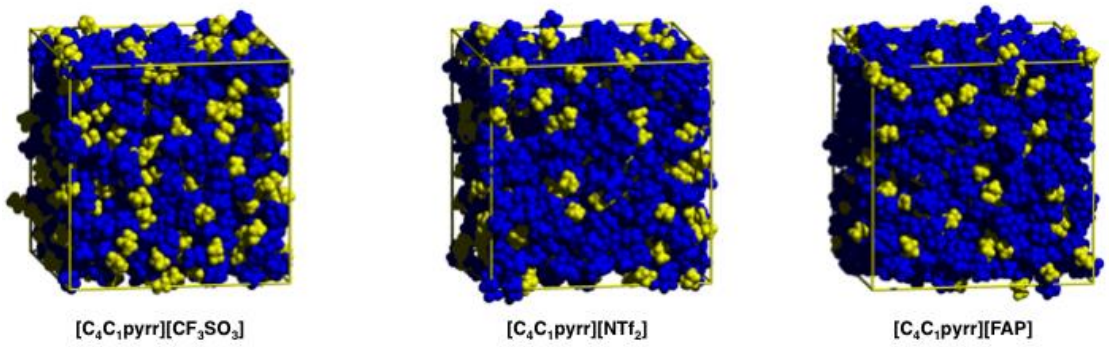

Figure 3. Snapshots of simulation boxes depicted using a coloring code to identify the polar (charged, depicted in blue) and non-polar (depicted in yellow) domains that are formed in the ionic liquids. The lengths of the boxes sides are given: a) $[C_4C_1pyrr][CF_3SO_3]$ l = 51.6 Å, b) $[C_4C_1pyrr][NTf_2]$ l = 52.2 Å, c) $[C_4C_1pyrr][FAP]$ l = 54.1 Å.

FIGURE 4

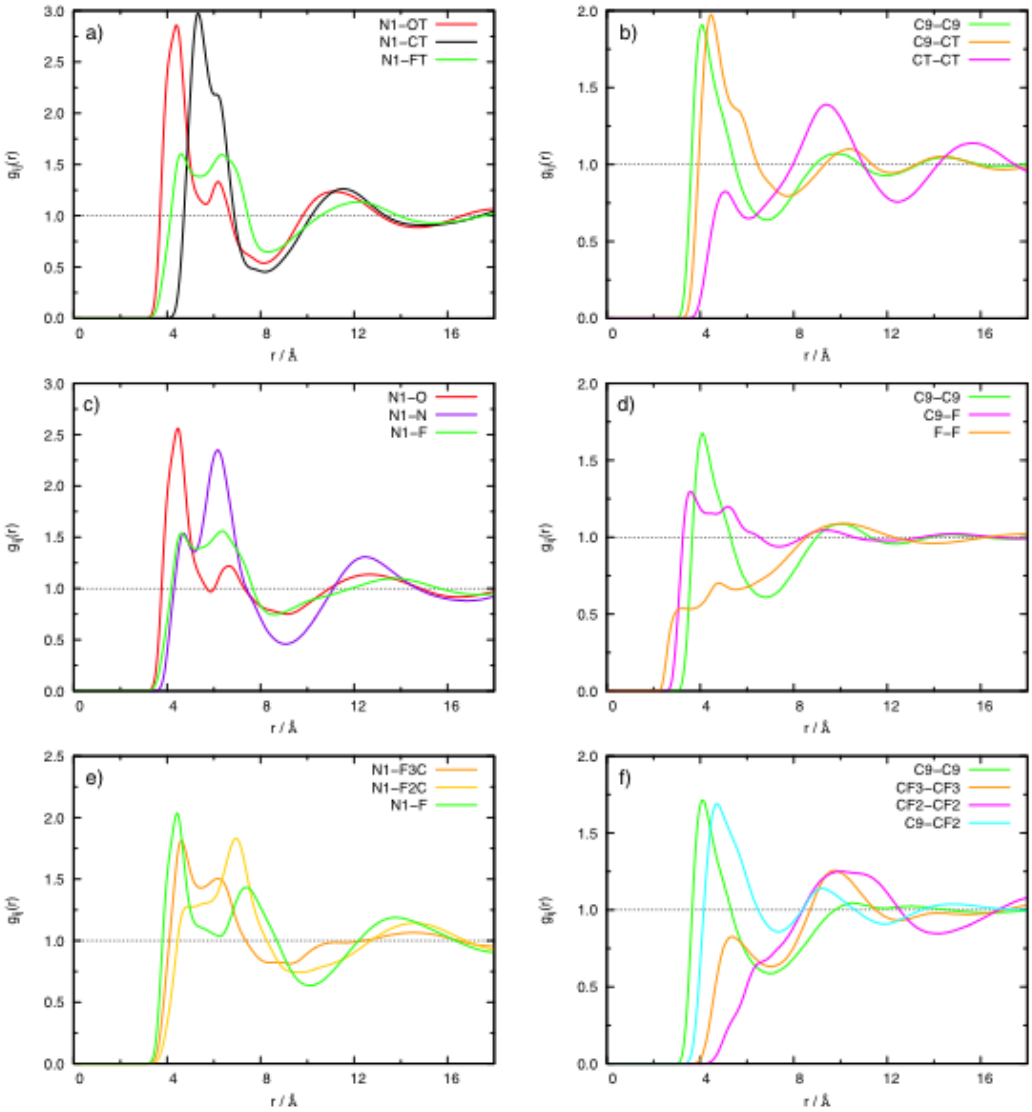

Figure 4. Site–Site Radial Distribution Functions (RDFs) between several representative atoms of the cations and anions: a) and b) 1-butyl-1-methylpyrrolidinium triflate, c) and d) 1-butyl-1-methylpyrrolidinium bis(trifluoromethanesulfonyl)imide and e) and f) 1-butyl-1-methylpyrrolidinium tris(pentafluoroethyl)trifluorophosphate. For nomenclature, please refer to Figure 1.

FIGURE 5

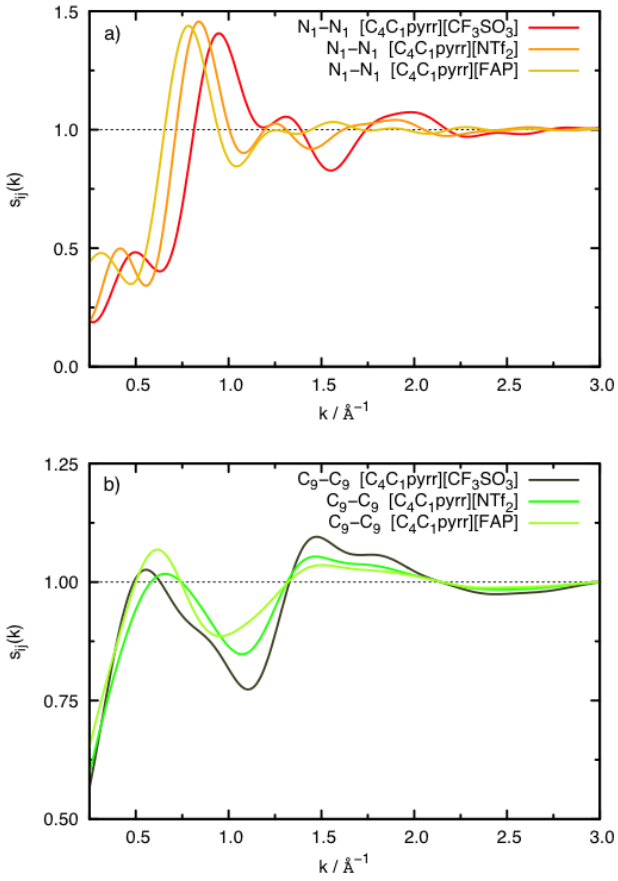

Figure 5. Static structure factors of representative atoms of the a) polar and b) non-polar regions calculated from radial distribution functions.

FIGURE 6

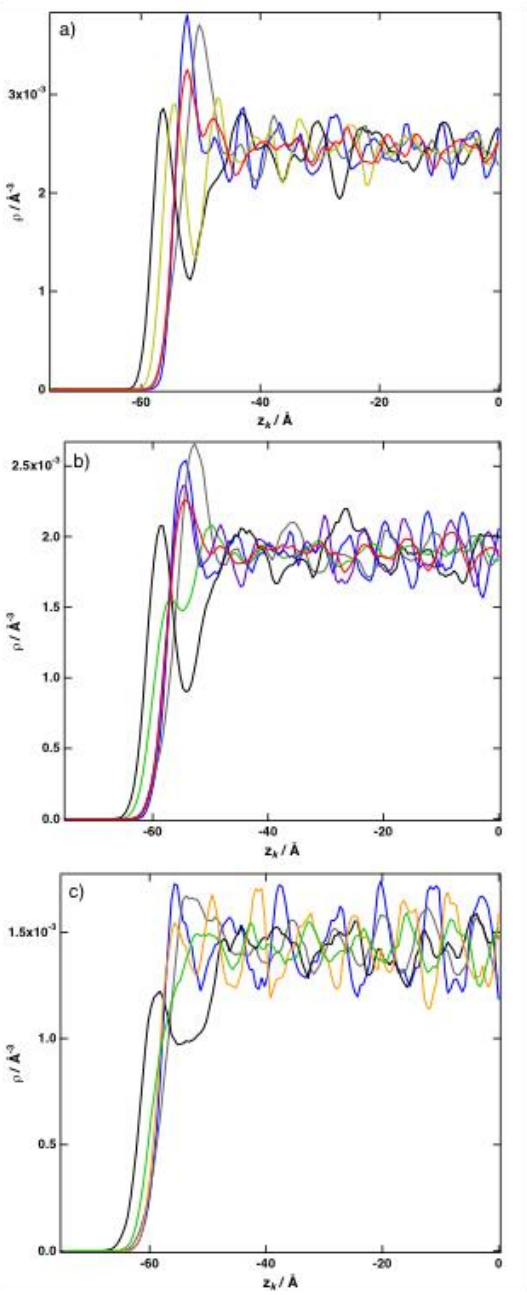

Figure 6. Number density profile of a) [C_4C_1pyrr][CF_3SO_3]: blue line: N1; grey line: C3,4; black line: C9; yellow line: CT; red line: OT b) [C_4C_1pyrr][NTf_2]: blue line: N1; grey line: C3,4; black line: C9; green line: F; purple line: N; red line: O c) [C_4C_1pyrr][FAP]: blue line: N1; grey line: C3,4; black line: C9; green line: CF3; orange line: P.

FIGURE 7

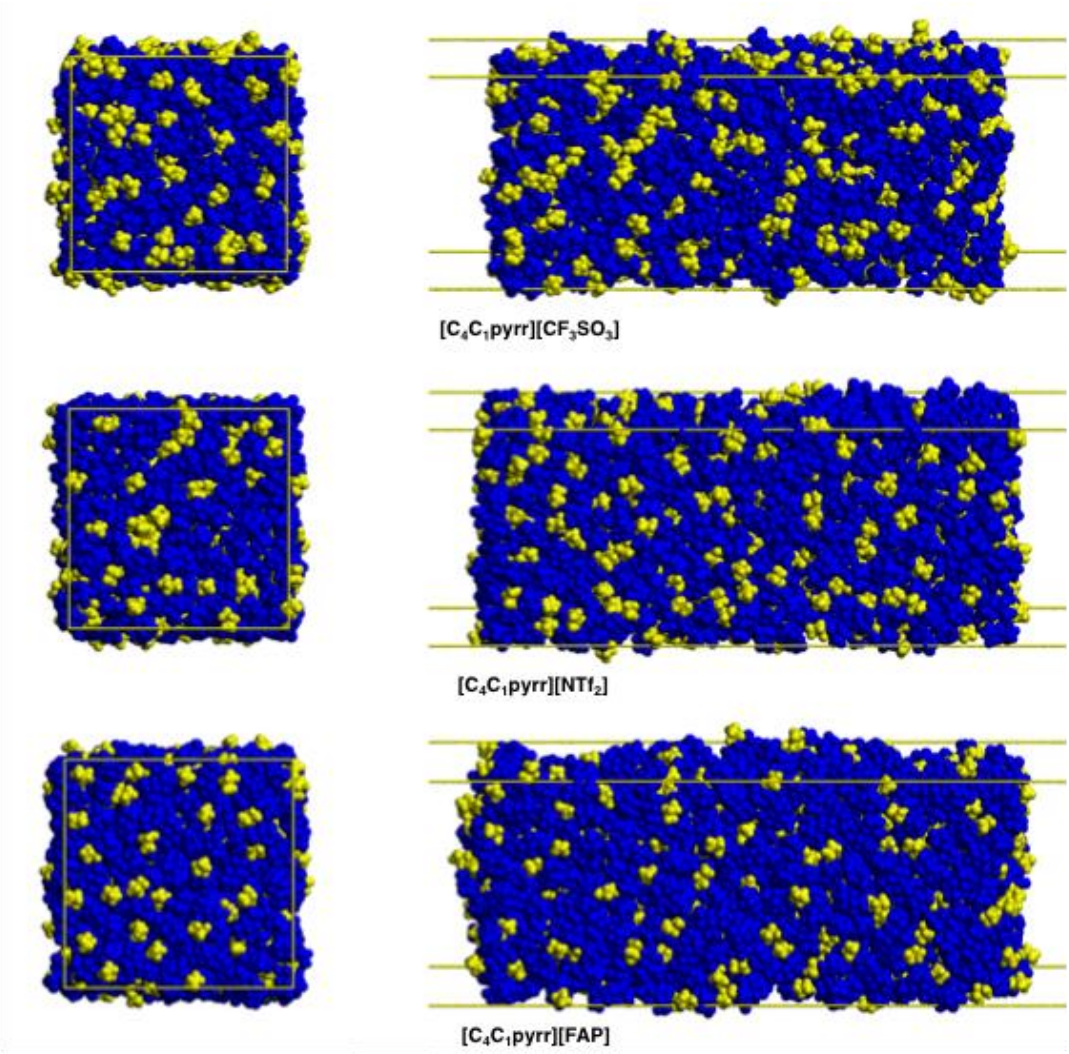

Figure 7. Snapshots of the simulation boxes. The high-charged regions are represented in blue and the low-charged regions in yellow.

FIGURE 8

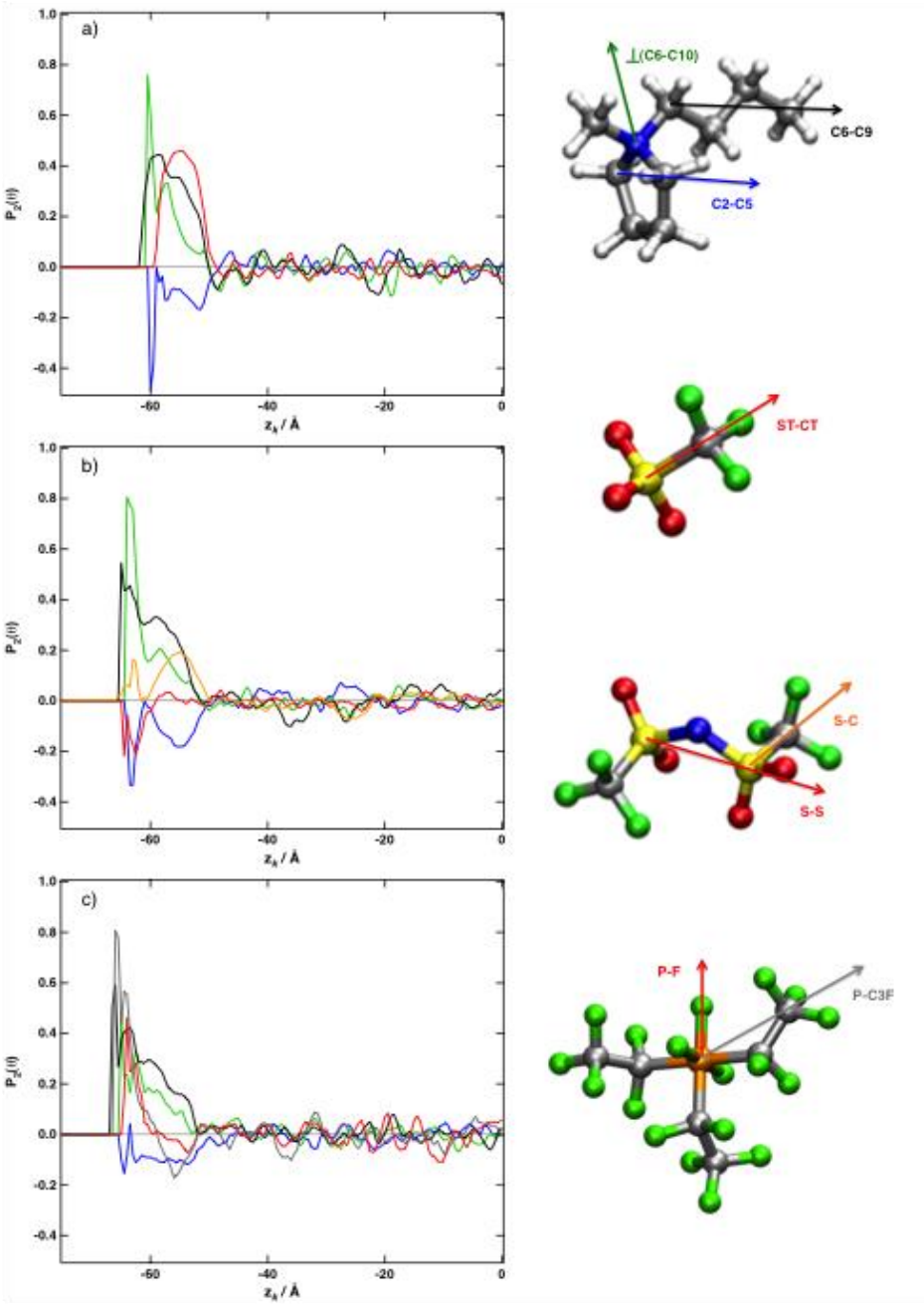

Figure 8. Orientational ordering parameter. θ is defined by the angle between the directional vectors and the surface normal. Blue line C2-C5 vector of the $[C_4C_1pyrr]^+$ cation; green line vector perpendicular to (C6-C10) pointing in the direction of N1 of the $[C_4C_1pyrr]^+$ cation; black line C6-C9 vector of the $[C_4C_1pyrr]^+$ cation. Panel a) $[C_4C_1pyrr][CF_3SO_3]$: red line ST-CT vector of the $[CF_3SO_3]^-$. Panel b) $[C_4C_1pyrr][NTf_2]$: red line S-S of the $[NTf_2]^-$ anion; orange line S-C of the $[NTf_2]^-$ anion. Panel c) $[C_4C_1pyrr][FAP]$: red line P-F vector of the $[FAP]^-$ anion; grey line P-C3F vector of the $[FAP]^-$ anion.

FIGURE 9

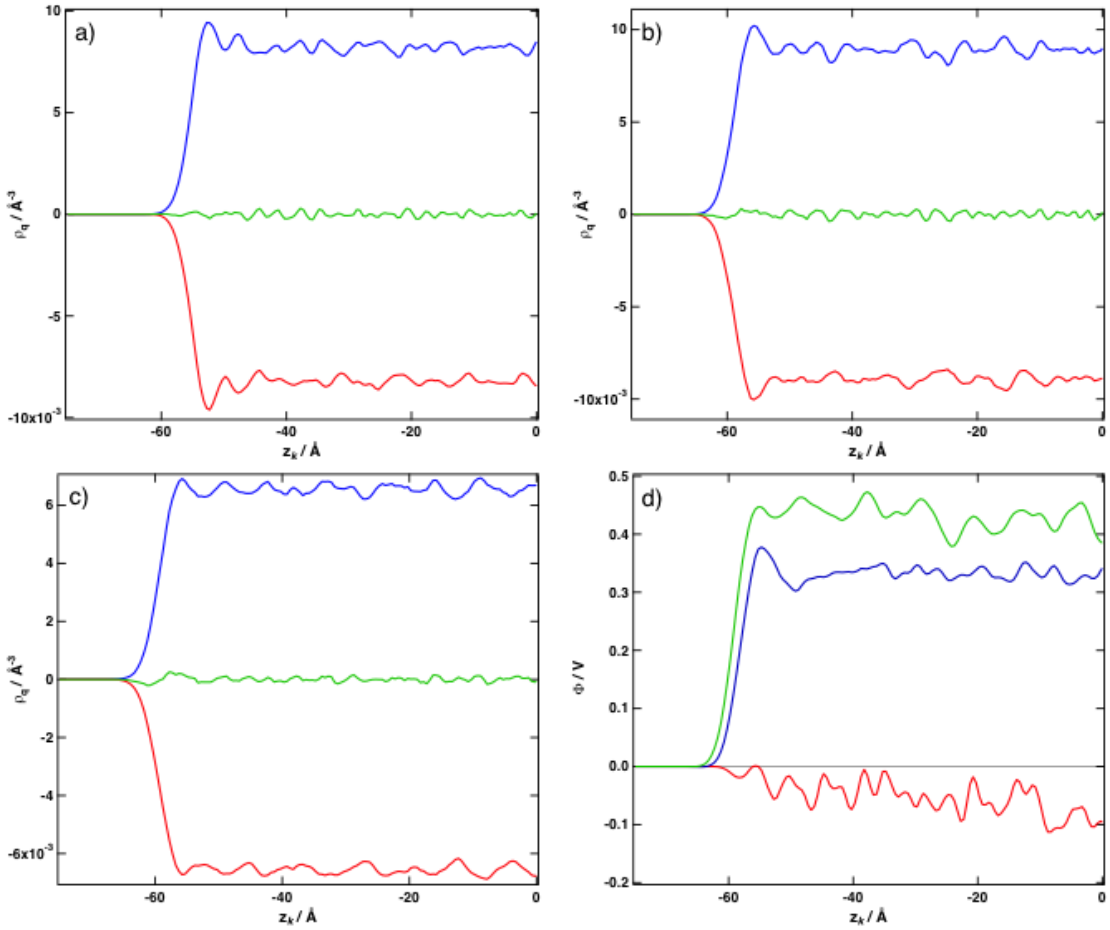

Figure 9. Charge density profiles for a) [C_4C_1pyrr][CF_3SO_3], b) [C_4C_1pyrr][NTf_2] and c) [C_4C_1pyrr][FAP]. Blue curves correspond to the cation, red curves to the anions and green curves to the sum of these two contributions. Panel d) electrostatic potential for [C_4C_1pyrr][CF_3SO_3]: red line; [C_4C_1pyrr][NTf_2]: blue line; [C_4C_1pyrr][FAP]: green line.

FIGURE 10

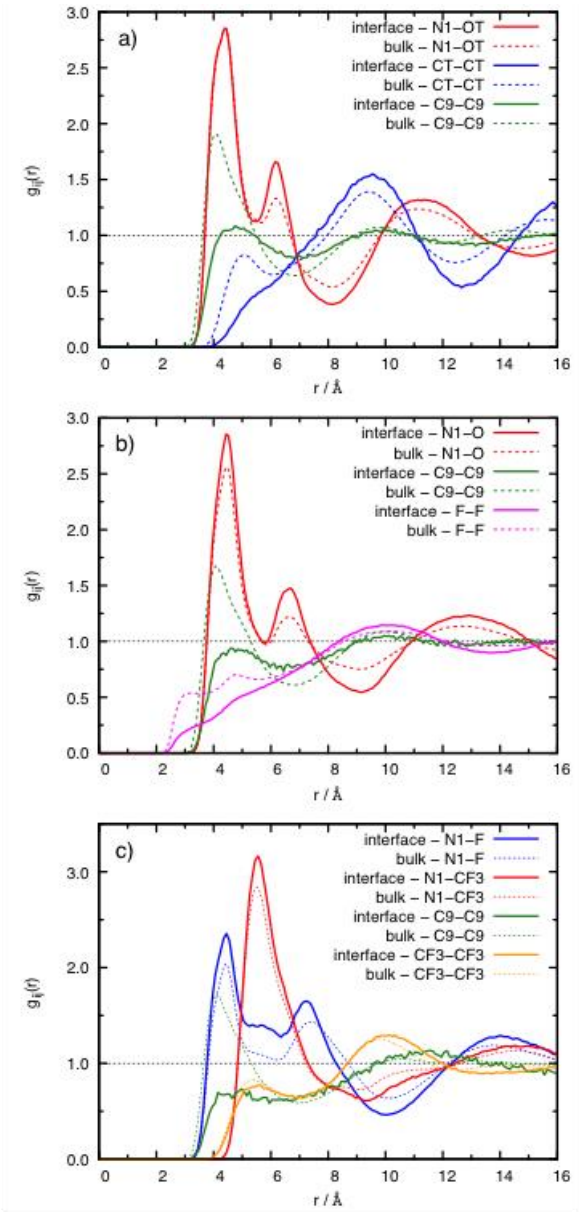

Figure 10. Tangential radial distribution functions (TRDF) of individual regions for several representative pairs of atoms in the interfacial (solid lines) and bulk regions (dashed lines): a) [C_4C_1pyrr][CF_3SO_3]: red line N1-OT; green line C9-C9; blue line CT-CT. b) [C_4C_1pyrr][NTf_2]: red line N1-OT; green line C9-C9; magenta line F-F. c) [C_4C_1pyrr][NTf_2]: red line N1-CF3; blue line N1-F; green line C9-C9; orange line CF3-CF3.

FIGURE 11

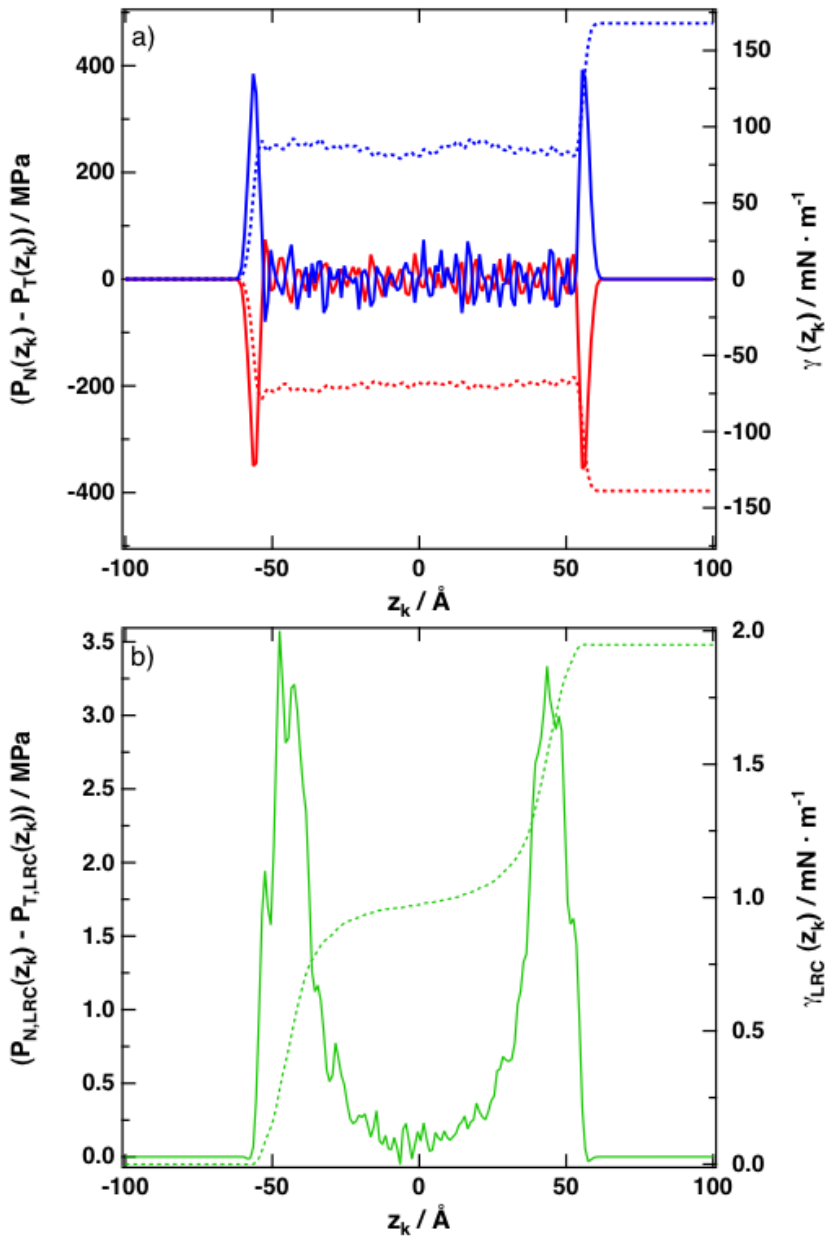

Figure 11. a) $p_N(z_k) - p_T(z_k)$ for the Lennard-Jones (red curve) and the electrostatic part of the potential (blue curve) as a function of z_k for $[C_4C_1pyrr][NTf_2]$. The dashed lines correspond to the integral as a function of z (right axis); b) $p_N(z_k) - p_T(z_k)$ for the long-range corrections as a function of z_k for $[C_4C_1pyrr][CF_3SO_3]$. The dashed lines correspond to the integral as a function of z_k (right axis).

Table 1. Length scales of the polar/non-polar domains obtained from analysis of the static structure factors.

Ionic liquid	Peak wavenumber / Å^{-1}	Length scale / Å
	Polar domains	
[C_4C_1pyrr][CF_3SO_3]	0.95	6.6
	0.50	12.6
[C_4C_1pyrr][NTf_2]	0.84	7.5
	0.43	15.1
[C_4C_1pyrr][FAP]	0.78	8.1
	0.32	19.6
	Non-polar domains	
[C_4C_1pyrr][CF_3SO_3]	0.56	11.2
[C_4C_1pyrr][NTf_2]	0.64	9.8
[C_4C_1pyrr][FAP]	0.61	10.3

Table 2. Surface Tension ($mN \cdot m^{-1}$) for the Studied Ionic Liquids Calculated from MD Simulations Using the Different Operational Expressions at T = 423 K[a].

	$[C_4C_1pyrr][CF_3SO_3]$	$[C_4C_1pyrr][NTf_2]$	$[C_4C_1pyrr][FAP]$
γ_{KB}	29.1 ± 3.5	30.3 ± 3.6	30.6 ± 3.7
γ_{IK}	27.5 ± 3.3	28.9 ± 3.5	30.2 ± 3.6
γ_{LRC}	1.95	1.9	1.87
$<\gamma>$	30.3 ± 3.5	32.5 ± 3.6	32.3 ± 3.7

[a] $<\gamma>$ is averaged over KB and IK methods.